



1

1
2
3
4
5
6
7
8
9
10
11
12
13
14
15
16
17
18
19
20
21
22
23
24
25
26
27
28
29
30
31
32
33
34
35
36
37
38
39
40
41
42
43
44
45
46
47
48

Coastal Sea Level rise at Senetosa (Corsica) during the Jason altimetry missions

Yvan Gouzenes¹, Fabien Léger¹, Anny Cazenave^{1,2}, Florence Biro¹, Pascal Bonnefond³,
Marcello Passaro⁴, Fernando Nino¹, Rafael Almar¹, Olivier Laurain⁵, Christian Schwatke⁴,
Jean-François Legeais⁶ and Jérôme Benveniste⁷

1. LEGOS, Toulouse; 2. ISSI, Bern; 3. Observatoire de Paris-SYRTE, Paris ; 4. TUM,
Munich; 5. Observatoire de la Côte d'Azur-Géoazur, Sophia-Antipolis; 6. CLS, Ramonville
St Agne; 7. ESA-ESRIN, Frascati.

10 January 2020

Corresponding author: Anny Cazenave (anny.cazenave@legos.obs-mip.fr)



49
50
51
52

53 **Abstract**

54 In the context of the ESA Climate Change Initiative project, we are engaged in a regional
55 reprocessing of high-resolution (20 Hz) altimetry data of the classical missions in a number of
56 world's coastal zones. It is done using the ALES (Adaptive Leading Edge Subwaveform)
57 retracker combined with the X-TRACK system dedicated to improve geophysical corrections
58 at the coast. Using the Jason-1&2 satellite data, high-resolution, along-track sea level time
59 series have been generated and coastal sea level trends have been computed over a 14-year
60 time span (from July 2002 to June 2016). In this paper, we focus on a particular coastal site
61 where the Jason track crosses land, Senetosa, located south of Corsica in the Mediterranean
62 Sea, for two reasons: (1) the rate of sea level rise estimated in this project increases
63 significantly in the last 4-5 km to the coast, compared to what is observed further offshore,
64 and (2) Senetosa is the calibration site for the Topex/Poseidon and Jason altimetry
65 missions, equipped for that purpose with in situ instrumentation, in particular tide gauges
66 and GNSS antennas. A careful examination of all the potential errors that could explain the
67 increased rate of sea level rise close to the coast (e.g., spurious trends in the geophysical
68 corrections, imperfect intermission bias estimate, decrease of valid data close to the coast and
69 errors in waveform retracking) has been carried out, but none of these effects appear able
70 to explain the trend increase. We further explored the possibility it results from real
71 physical processes. Change in wave conditions was investigated but wave set up was
72 excluded as a potential contributor because of too small magnitude and too localized in the
73 immediate vicinity of the shoreline. Preliminary model-based investigation about the
74 contribution of coastal currents indicates that it could be a plausible explanation of the
75 observed change in sea level trend close to the coast.



76

77 **1. Introduction**

78 Since the early 1990s, satellite altimetry provides invaluable observations of the global mean
79 sea level and its regional variability. In the recent years, this data set has generated an
80 abundant literature on the processes causing sea level change at global and regional scales, as
81 well as on closure of the sea level budget (e.g., Church et al., 2013, Stammer et al., 2013,
82 Dieng et al., 2017, Nerem et al., 2018, WCRP, 2018, SROCC, 2019). In addition to the global
83 mean rise and superimposed regional trends, changes in small scale processes such as local
84 atmospheric effects, baroclinic instabilities, coastal trapped waves, shelf currents, waves,
85 fresh water input from rivers in estuaries, can substantially modify the rate of sea level change
86 at the coast compared to open sea regions (Woodworth et al., 2019, Melet et al., 2018,
87 Piecuch et al., 2018, Dodet et al., 2019, Durand et al., 2019). In addition, ground subsidence
88 may amplify the rate of sea level change at the coast (Woppelmann and Marcos, 2016). In
89 terms of societal impacts, what really matters in the coastal zone is indeed the sum of the
90 global mean sea level rise plus the regional trends and the local processes.

91 Up to recently, due to land contamination of radar echoes and less precise geophysical
92 corrections, classical altimetry did not provide reliable sea level data in a band of 10-15 km
93 along coastlines. However different studies have shown that using adapted reprocessing of
94 altimetry measurements and improving geophysical corrections allows retrieving a large
95 amount of valid sea level close to the coast (e.g., Cipollini et al., 2018, Passaro et al., 2015,
96 Marti et al., 2019). In addition, despite having a much higher noise level than the classical 1
97 Hz altimetry data, high-resolution 20 Hz measurements allow to recover more information on
98 coastal sea level variations (Birol and Delebecque, 2014, Leger et al., 2019).

99 In the context of the Climate Change Initiative (CCI) project of the European Space
100 Agency (ESA), we have initiated a reprocessing of high-resolution (20 Hz) altimetry data of
101 the Jason-1 and Jason-2 missions along coastal zones of Western Africa, Northern Europe and
102 Mediterranean Sea. The ALES (Adaptive Leading Edge Subwaveform) retracker (Passaro et
103 al., 2014) was applied to estimate the satellite-sea surface distance (called range) which was
104 further combined with the X-TRACK processing chain dedicated to improve geophysical
105 corrections at the coast (Birol et al., 2017). This allowed us to derive along-track sea level
106 anomaly (SLA) time series (Leger et al., 2019) from which coastal sea level trends were
107 estimated. Results show that in a number of sites, coastal sea level rates computed over a 14-
108 year time span (2002-2016) significantly deviate from the open ocean rate within 5 km to the
109 coast (Marti et al., 2019).



110

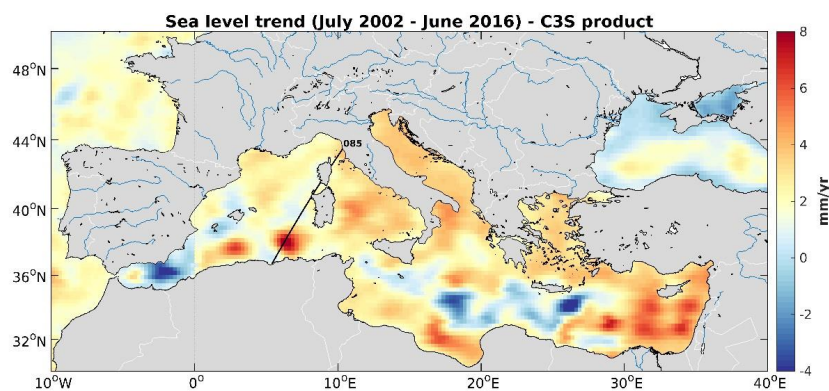
111 In the present study, we focus on a particular site, Senetosa, located south of Corsica in the
112 Mediterranean Sea (41°N, 8°E), for two reasons: (1) in this region, the computed rate of sea
113 level rise increases significantly in the last 3-5 km to the coast, and (2) there is a Jason
114 satellite track that crosses land at Senetosa, a calibration site for altimetry missions chosen
115 since the launch of the Topex/Poseidon mission in 1992 and equipped for that purpose with in
116 situ instrumentation, in particular tide gauges and GNSS antennas (Bonnefond et al., 2019).
117 This calibration site provides an independent reference to explore the near-shelf signal
118 observed in altimetry data.

119

120 2. Data and method

121 As presented in detail in Marti et al. (2019) and Léger et al. (2019), here we use the regional
122 X-TRACK/ALES along-track 20 Hz SLA data derived from Jason-1 and Jason-2 missions
123 (DOI: 10.5270/esa-sl_cci-xtrack_ales_sla-200201_201610-v1.0-201910). This product is
124 based on new ranges and new sea state bias corrections estimated using the ALES retracker,
125 and further combined with the X-TRACK software developed at CTOH (Center of
126 Topography of the Ocean and the Hydrosphere) at LEGOS (Laboratoire d'Études en
127 Géophysique et Océanographie Spatiales). The 14-year long 20-Hz SLA time series are
128 obtained by projecting the sea surface height data onto 'mean' reference ground tracks, after
129 adjusting for the regional intermission bias between the Jason-1 and Jason-2 missions. SLAs
130 have been further averaged on a monthly basis at every 20 Hz point and an editing has then
131 been performed to remove outliers (details in Marti et al., 2019). In this study we focus on
132 the section of Jason track 85 located off the southwestern coast of Corsica island (western
133 Mediterranean Sea) (see Fig. 1).
134

135





136

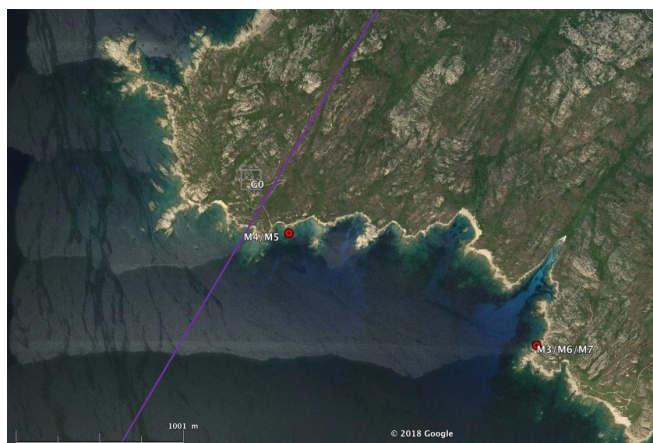
137 *Fig. 1: Location of the Jason track 85 crossing Corsica at the Senetosa site. The background*
138 *maps shows sea level trends over 2002-2016, based on gridded altimetry data from the*
139 *Copernicus Climate Change Service (C3S).*
140

141 3. The Senetosa calibration site

142 Since 1998, Senetosa is operating a calibration/verification site of the Topex/Poseidon and
143 Jason missions with the support of CNES (Centre National d'Études Spatiales, France),
144 NASA (National Aeronautics and Space Administration, USA) and the Observatoire de la
145 Côte d'Azur (France). It is equipped with different in situ instrumentation, including weather
146 stations, several tide gauges and GNSS antenna. Since 1998, this calibration site has been
147 widely used to validate the altimetry-based sea surface height data (Bonnetfond et al., 2003a,b,
148 2010, 2011). Fig.2 is a Google Earth image of the coast, showing the geographical
149 configuration of the Senetosa calibration site, with the location of the tide gauges, the GNSS
150 antenna and the Jason track. Three tide gauges were operating during our study period (M3,
151 M4 and M5). M4 and M5 are at the exact same location, a few tens of cm apart, on the
152 western part of the coastline while M3 is located about 1.7 km eastward of M4/M5.
153 According to the Google image of the coastline configuration shown on Fig.2, we note that
154 M4/M5 are sheltered from northwestward wind forcing while M3 is more exposed to open sea
155 conditions from the west.

156 Vertical land motion time series are available from the GNSS reference receiver located close
157 to the lighthouse (G0 reference marker in Fig.2). The tide gauges have been regularly leveled
158 relatively to the G0 reference marker with no relative motion detected so far at the millimeter
159 level over 10 years. Trends in sea level and vertical land motions derived from these
160 instruments at Senetosa are discussed in section 5.

161



162



163
164
165
166
167
168
169
170
171

Fig. 2: © Google Earth image of the Senetosa calibration site. The two tide gauge sites (referred as M4/M5 and M3) are shown by the red dots. The G0 reference marker (G0) is indicated by a grey square and the Jason ground track by a purple line.

172 **4. Analysis of the coastal sea level trends off Senetosa**

173 **4.1 Coastal sea level trends derived from altimetry data**

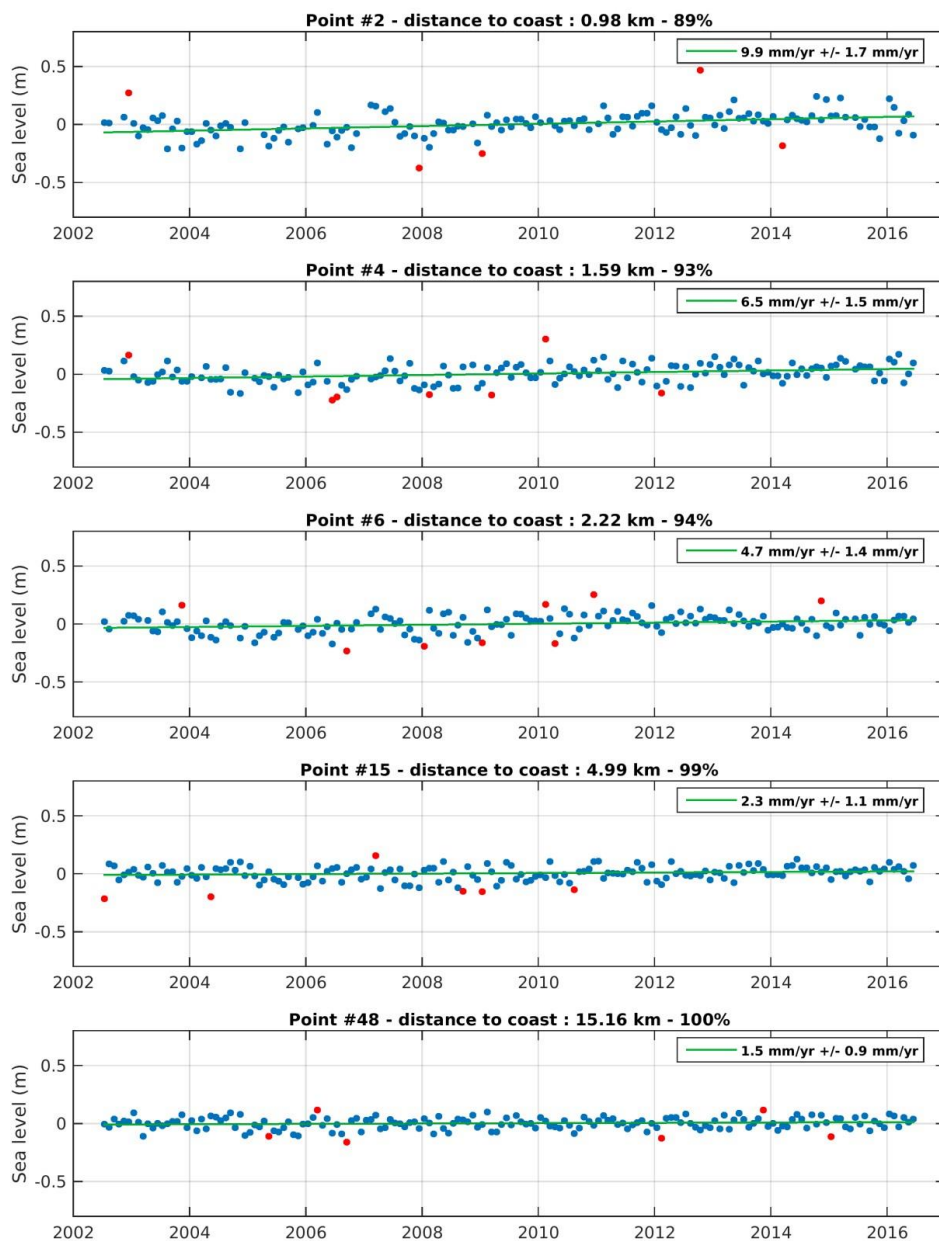
174 Following the data processing described above, we focus on monthly SLA time
175 series sampled at 20 Hz (~350 m in the along-track direction), from 15 km offshore
176 to the

177 coastline. Examples of along-track SLA time series at coastal points, located at 1 km, 1.6
km, 2.2 km, 5 km and 15 km from the coast respectively, are shown in Fig.3.



178
179

7



180
181
182

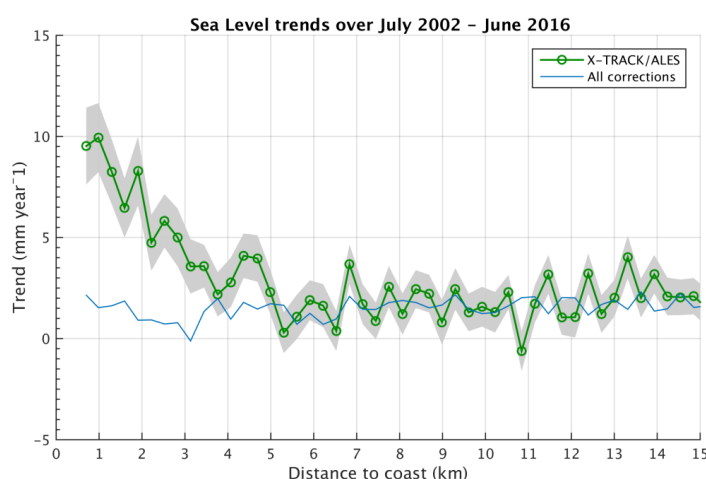
183 *Fig. 3: Examples of sea level anomalies time series for 20-Hz points located at different*
184 *distances from the coast. The distance to coast, percentage of valid data and sea level trends*
185 *are indicated on each plot. The green curve is the regression line adjusted to the data. The*
186 *red points on the time series correspond to outliers detected using a simple 2-sigma filter*
187 *(sigma corresponding to the SLA standard deviation). These are not considered to compute*
188 *the regression line.*



189
190
191
192

193 For each 20 Hz point, we have then computed the regression line of the resulting SLA time
194 series and the associated standard deviation (1-sigma) to estimate sea level trends over the
195 study time span. Fig.4 shows the corresponding along track sea level trends as a function of
196 distance to the coast (from 15 km offshore).

197
198
199
200
201
202
203
204
205
206
207
208
209
210
211
212
213
214
215
216
217



218
219
220
221
222

Fig. 4: Altimetry-based sea level trends around Senetosa as a function of distance to the coast . Shaded area corresponds to trend uncertainty range. The light blue curve is the sum of trends in individual corrections.

223
224
225
226
227

Fig.4 shows that beyond ~ 5 km from the coast towards the open sea, the trend over 2002-2016 is relatively stable and on average on the order of 2-3 mm/yr. High frequency oscillations around this value are observed between adjacent points but these are likely due to noise and we note they are of the same order of magnitude or only slightly larger than the standard deviation of trend estimates at each point (of ~1.5 mm/yr).

228
229
230

Fig.4 also shows an almost continuous increase in the trend in the last ~4-5 km to coast. The corresponding trend uncertainties (standard deviation) are not significantly larger than offshore (<2 mm/yr).



231

232 4.2 Robustness of the computed coastal trends

233 In coastal areas, important limitations to recover precise sea surface height from altimetry
234 data come from inaccuracies in some of the applied geophysical corrections (e.g. sea state
235 bias, wet tropospheric correction, dynamical atmospheric correction and ocean tides) and
236 from the distorted shape of the radar waveforms as the satellite approaches land (see for
237 example Vignudelli et al., 2011 for a complete review on the issues of coastal altimetry). The
238 corresponding altimetry measurements are often discarded by the processing chains or flagged
239 in the data sets but remaining errors can impact the sea level trend estimates located near the
240 coastline. The latter can also be impacted by the lower percentage of valid data in the coastal
241 zone, as well as by the uncertainty in the bias estimate between the two successive missions
242 Jason-1 and Jason-2. In order to check whether the sea level trend increase close to the coast
243 reported in section 4.1 is associated to one of these factors, we examine each of them
244 independently.

245

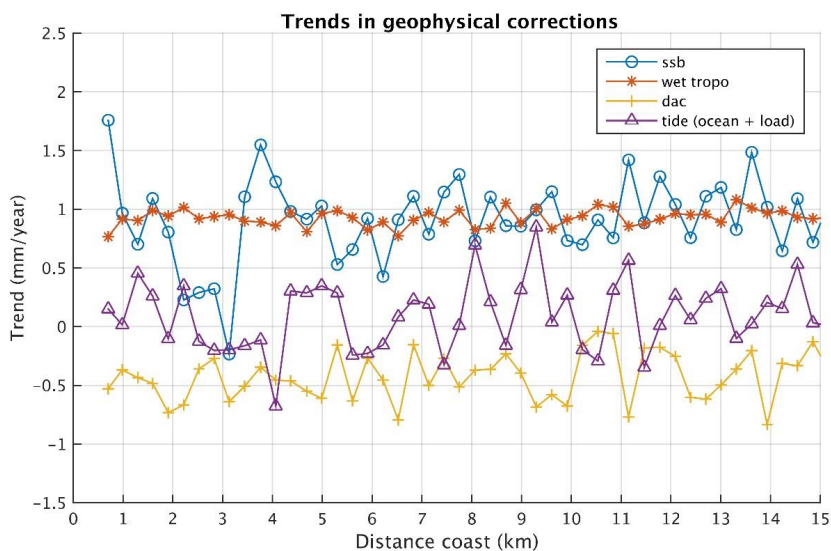
246 4.2.1 Coastal errors in the geophysical corrections

247 We first computed and plotted the geophysical correction trends as a function of distance to
248 the coast for the sea state bias (ssb), wet atmospheric correction, atmospheric loading (called
249 DAC- dynamic atmospheric correction-) and ocean and loading tide correction (Fig.5).

250

251

252



253

254
255
256
257

258 *Fig. 5: Trends in the geophysical corrections (sea state bias/ssb, wet tropospheric correction,*
259 *dynamic atmospheric correction/dac, ocean tide plus ocean loading tide) as a function of*
260 *distance to coast. Note that the vertical scale is different from Fig.4.*

261

262 Trends in the geophysical corrections are rather small and their amplitude in the range +/- 1
263 mm/yr, except for the ssb that shows a larger trend within 4 km to coast, but always less than
264 2 mm/yr. It is worth mentioning that the ssb is a function of significant wave height (SWH)
265 and backscatter coefficient (both related to wind speed). In the ALES retracking the ssb is
266 recomputed for each 20-Hz point. So a trend in ssb may be due to either a different behavior
267 of the SWH and wind speed at the coast, or to changes in backscatter properties.

268 The sum of these geophysical correction trends is plotted in Fig.4 (blue line). Even if the
269 geophysical corrections, and especially the ssb, are more uncertain close to the coast, Fig. 4
270 suggests that the continuous increase in the sea level trends observed in the last ~4 km to the
271 coast may not be due to trends in the geophysical corrections. It remains that the empirical
272 formulation used for the ssb correction may not be valid close to the coast where waves could
273 has a different behavior compared to the open sea. This will be discussed in section 6.1.

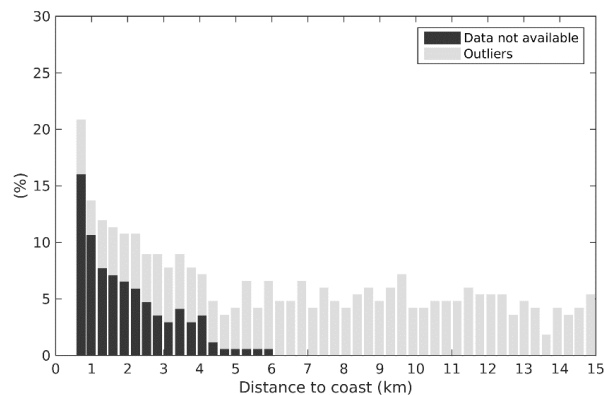
274

275 4.2.2 Coastal changes in the percentage of valid data

276 We next examined the possible impact on the trend estimation of the decrease in valid data in
277 the last 3-4 km to coast. The original percentage of valid data at each 20-Hz point decreases
278 with distance to the coast. It is shown in Fig.6a. If we keep the same lesser percentage of valid
279 data for all points, then only 80% of the original data set are left everywhere (Fig. 6b).

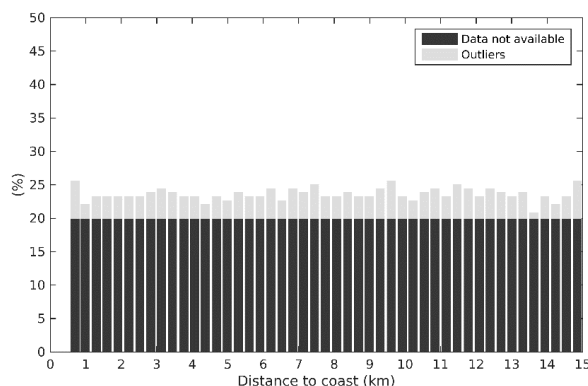
280

281 (a)



282
 283
 284

(b)

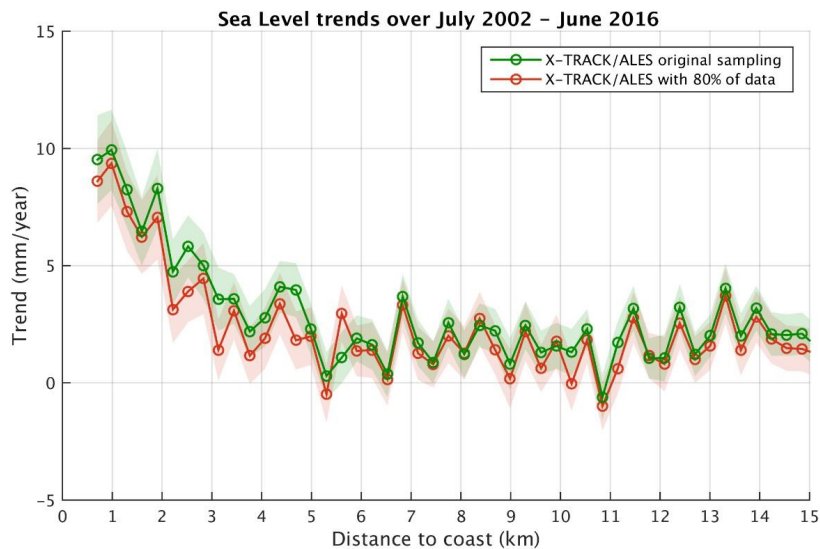


285
 286
 287
 288
 289
 290
 291
 292
 293
 294
 295
 296
 297
 298
 299
 300
 301
 302
 303

Fig. 6: (a) Percentage of missing points for the original data set. (b) Percentage of missing points for the data set where only common time series are kept.

304
 305
 306
 307
 308
 309
 310
 311
 312
 313
 314

The along-track sea level trends were recomputed with the new sampling (80% of the original data kept) (Fig.7). For comparison, in Fig.7 we superimpose the trends computed with the original sampling. Trends compare well in both cases. Even if the trend values are slightly lower in the band 0-5 km, keeping only 80% of the valid data does not change significantly the coastal trend behavior. We then conclude that the lower amount of valid near-shore altimetry data does not explain the trend increase observed as the distance to the coast decreases.



315



316
317
318
319
320

321 *Fig. 7: Sea level trends as a function of distance to the coast with the original data set (green*
322 *curve) and new sampling (80% of original data kept; red curve).*

323
324

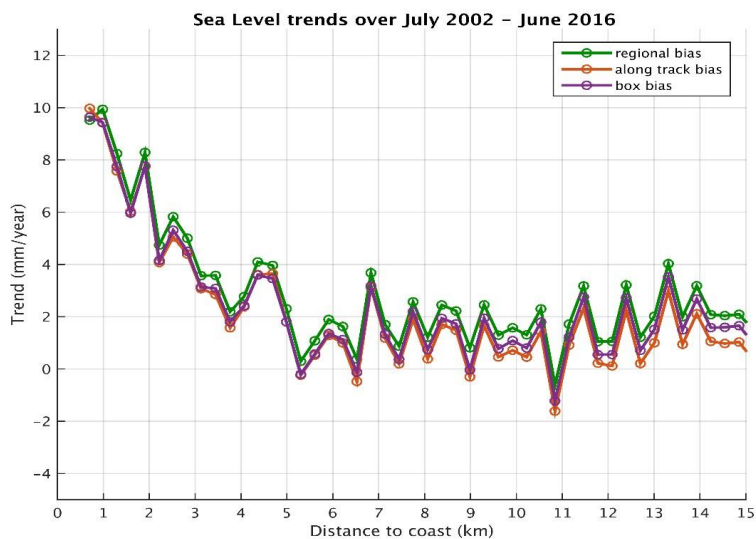
325 4.2.3 Effect of intermission bias estimation

326 As discussed in detail in Marti et al. (2019), in the X-TRACK/ALES sea level product, the
327 bias applied to combine the Jason-1 and Jason-2 data in a single sea level time series was
328 estimated at a regional scale. In the case of our study region, it was estimated over the whole
329 Mediterranean Sea. In order to investigate a possible impact of this approach on the sea level
330 trend estimates, we tested other bias calculation methods. We first recomputed the
331 intermission bias along the Jason track 85 (using only measurements of this particular track).
332 In another test, the bias was computed from data included in a 1x1 degree box around the
333 Senetosa site. The sea level trends derived from the corresponding Jason-1 and Jason-2 time
334 series are shown in Fig. 8a for these two cases, superimposed to the regional bias case shown
335 in section 4.1. Here again, we can see that there is almost no difference between the results of
336 the three approaches, indicating that inadequate intermission bias estimate does not explain
337 the coastal trend increase. To complete these tests, we also recomputed SLA trends as a
338 function of distance to coast using as reference a local geoid computed for altimetry mission
339 calibration purposes (P. Bonnefond, personal communication). Fig.8b shows the geoid profile
340 together with the along-track mean sea surface computed with the altimetry data, as a function
341 of latitude. Both references compare well. Thus, as expected, exactly the same trend increase
342 behavior as a function of distance to coast is observed when the reference geoid is used
343 (figure not shown as it is similar to Fig.4). We conclude that the reference has no impact
344 on the computed trends.



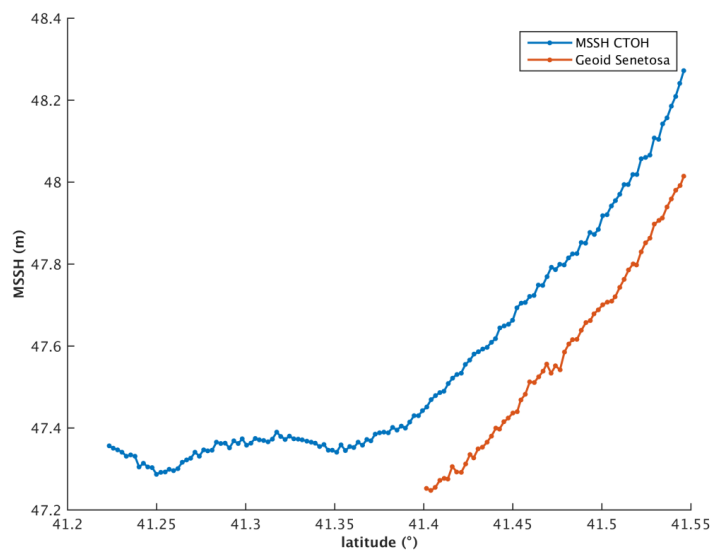
345

346 (a)
347
348



349
350
351
352
353

354 (b)
355
356
357



358
359
360

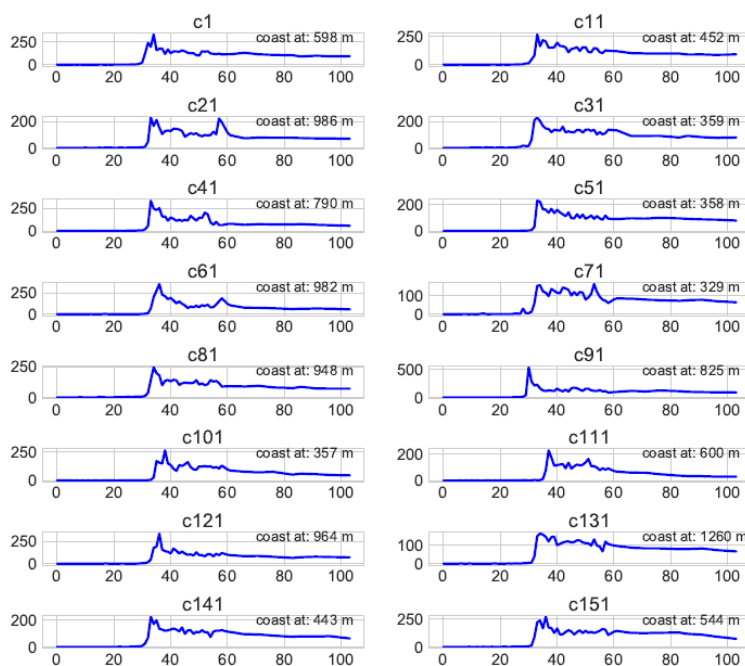
361 *Fig. 8: (a) Sea level trends as a function of distance to the coast for three different*
362 *intermission bias estimates. (b) Geoid and altimetry-based along-track mean sea surface*
363 *profiles as a function of latitude.*

364
365

366 4.2.4 Coastal altimetry waveforms and range values near Senetosa

367 In another series of tests, we examined the shape of the radar waveforms at 20 Hz points as a
368 function of distance to coast, considering a few Jason cycles taken at random. An example is
369 shown in Fig. 9 for a point located between the coast and 2 km offshore. Fig.9 shows that at
370 the Senetosa site, the leading edge of the coastal radar echo is generally well defined,
371 suggesting that a robust determination of the range is possible very close to the coast.

372
373



374
375

376
377 *Fig. 9: Observed radar waveforms at points close to the coast for a series of Jason cycles*
378 *(numbers on each plot refer to cycle number).*

379

380 To investigate this further, we tried to assess the reliability of successive 20-Hz ALES-based
381 range data very close to the coast. The waveform amplitude represents the radar power as a



382

383 function of time. For Jason-2, time is discretized into 104 successive ‘gates’. Knowledge of
384 the orbit and radar footprint allows by simple geometric analysis to associate a point on
385 ground (pixel) to a given gate. A numerical simulation has been performed for that purpose
386 (assuming flat land) in order to produce range maps for the Jason track 85, with the goal of
387 precisely locating the point on ground corresponding to the measured waveform. This is
388 illustrated on Fig. 10a and Fig. 10b, showing the geographical configuration and associated
389 radar waveforms for two range measurements located at 0.53 km and 1.4 km distance from
390 coast. The range measurement deduced from the waveform corresponds to the center of the
391 circle representing the radar footprint on the range map.

392

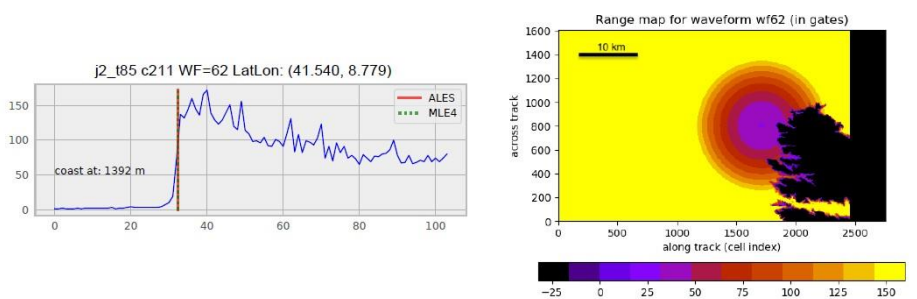
393

394

395

396

(a)

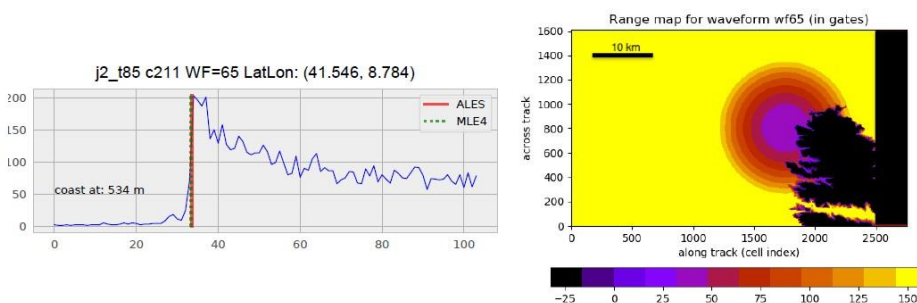


397

398

399

(b)



400

401

402 *Fig. 10: (a) Radar waveform as a function of gate number (left) and configuration of the*
403 *radar footprint on ground (right) at 1.4 km from coast. (b) Same as (a) at 0.5 km from coast.*

404

405

406 Although these simulations represent an ideal case of smooth sea state and flat land,
407 Fig. 10a,b shows that even at the closest point to coast (0.5 km), the leading edge of the return



408

409 waveform still corresponds to a reflection of the radar signal on water. This suggests that it is
410 theoretically possible to retrieve valid sea level information up to 0.5 km to the coast. One
411 may argue that because the land at Senetosa has some elevation, the real radar echo is partly
412 contaminated by land reflection at distances larger than the theoretical footprint, even if there
413 is no wave. However, considering that the real waveform has a leading edge, and that
414 the retracker is able to follow it, we conclude that the trends reported on successive 20-Hz
415 points are not spurious. Besides, if the retracker was corrupted by inhomogeneous backscatter
416 properties within the satellite footprint, these should be random (e.g., Passaro et al. 2014).
417 Finally, 20-Hz waveforms being independent samples, if the retracker is wrong and produces
418 spurious trends, the latter also would be random. Thus, we should not see a continuous trend
419 increase over several consecutive points.

420

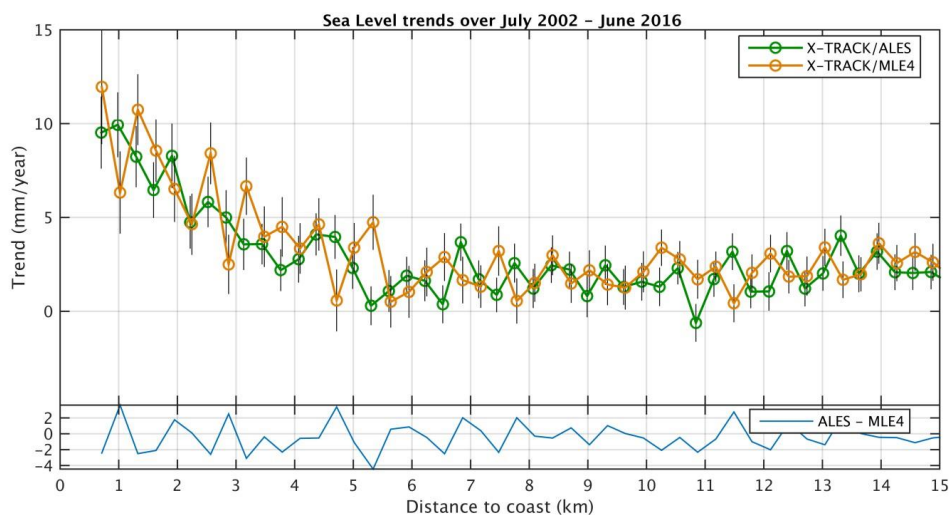
421 4.2.6 Comparison between ALES and MLE4 retrackers

422 Finally, we performed the same analysis (computation of sea level trends as a function of
423 distance to the coast) using SLA data computed with the classical MLE4 retracker (used for
424 the standard Geophysical Data Records production, https://www.aviso.altimetry.fr/fileadmin/documents/data/tools/hdbk_tp_gdrm.pdf). MLE4-
425 based trends over the 14-year time span are shown in Fig. 11, on which are superimposed the
426 ALES-based trends, for comparison. We note that MLE4 gives noisier results than ALES,
427 especially at distances less than ~5 km to the coast, but the increase in trends in the last ~4-5
428 km to the coast is still well visible. This clearly means that the trend increase is not an artifact
429 due to the use of the ALES retracker.
430



431
432

17



433
434
435
436

437 *Fig. 11: Sea level trends as a function of distance to the coast for MLE4 (orange dots) and*
438 *ALES (green dots)-based SLA data. Vertical bars correspond to trend errors (1-sigma). The*
439 *light blue curve at the bottom of the panel represents the difference between ALES-based and*
440 *MLE4-based trends.*

441
442
443

444 To summarize, from all the tests presented above, we can conclude that the increase in
445 altimetry sea level trend observed in the last 4-5 km to the coast is not correlated with errors
446 in the geophysical corrections, is not explained by the loss of valid data, nor the presence of
447 spurious waveforms or by the intermission bias. Furthermore, the calculated trends are robust
448 to change in retracker, since instead of using ALES, we also used the standard high-frequency
449 MLE4 retracker. The corresponding time series still show the same trend behavior (although
450 with noisier results).

451

452 **5. Comparison with the sea level trend derived from tide gauges records**

453
454
455
456
457
458

It is very classical to validate altimetry-based sea level data by comparing with tide gauge records. The availability of tide gauge records at the Senetosa site is a good opportunity to do so. Tide gauge data have been provided by the Observatoire de la Côte d'Azur (Géoazur laboratory) and downloaded from www.aviso.altimetry.fr/en/data/calval/in-situ/absolute-calibration/download-tide-gauge-data.html. The high-frequency tidal signal and the atmospheric forcing effect have been removed (using the same DAC correction as for the

459

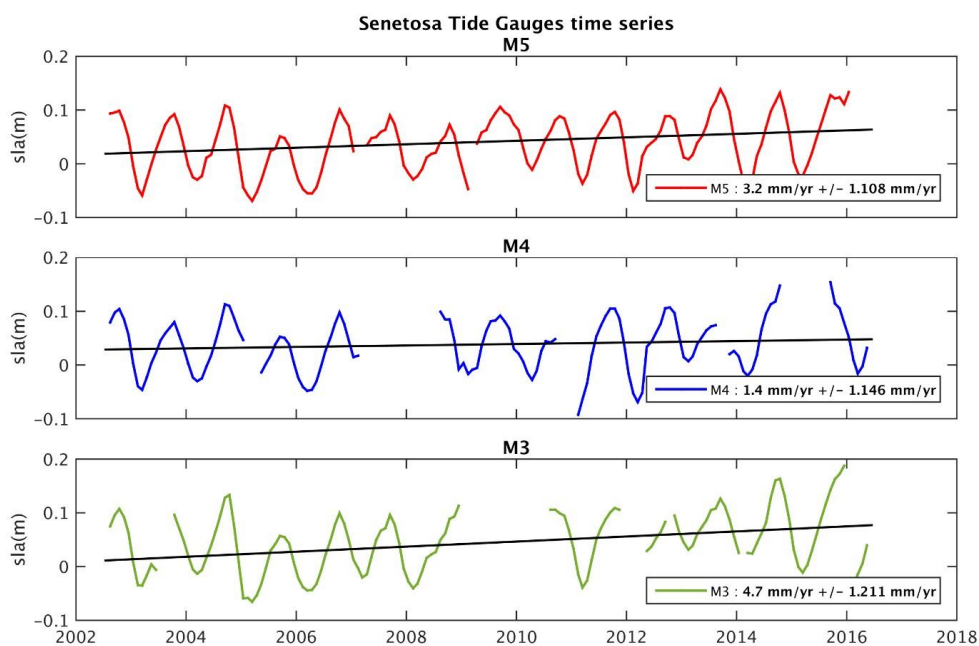
460 altimetry data). The time series have been further smoothed on a monthly basis. The
461 corresponding tide gauge time series over 2002-2016, for the M3, M4 and M5 tide gauges, are
462 shown in Fig. 12a and 12b, with and without the seasonal cycles.

463

464

465

(a)

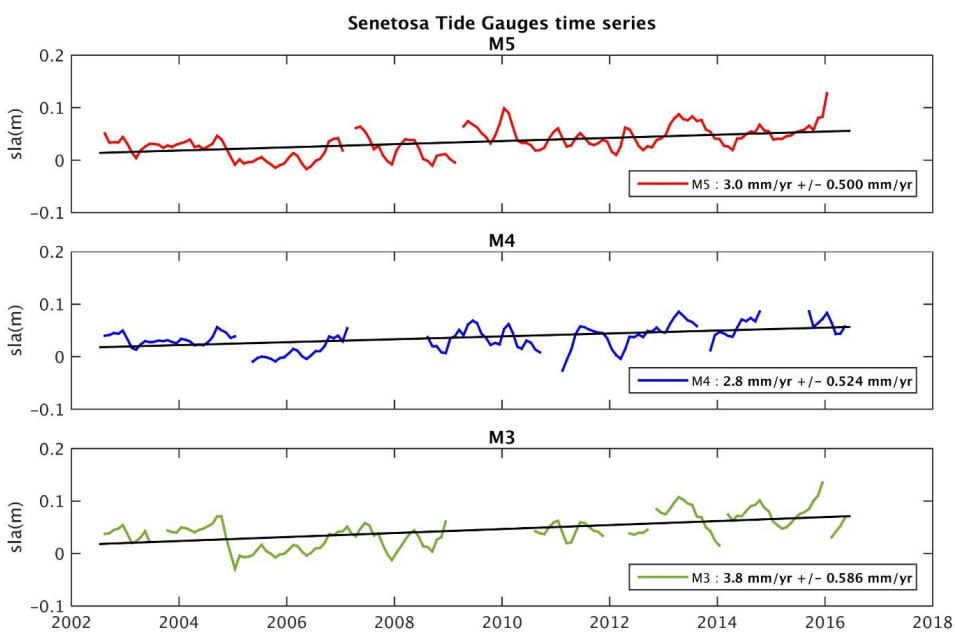


466

467

468

(b)



469

470
471
472
473
474
475
476
477
478
479
480
481
482
483
484

Fig. 12: Sea level time series based on in situ tide gauges measurements at the M3, M4 and M5 sites over 2002-2016. (a) With the seasonal cycle. (b) Without the seasonal cycle.

From these time series, we computed linear trends over the same period as for the altimetry data. These are gathered in Table 1 for the two cases (with and without the seasonal cycle). In Bonnefond et al. (2019), it was shown that when making differences between tide gauges sea level measurements, there is no systematic trend between the tide gauge time series since 2001 (below 0.1 mm/yr), well within the trend uncertainties. The GNSS-based vertical land motion (VLM) at Senetosa (estimated in Bonnefond et al., 2019) is also shown. VLM is small at Senetosa, less than 0.3 mm/yr.

Tide Gauge	Tide gauge trend (mm/yr) (with seasonal cycles)	Tide gauge trend (mm/yr) without seasonal cycles	GNSS VLM (2003-present) (mm/yr)
M3	4.7 +/- 1.2	3.8 +/- 0.6	0.28 +/- 0.05
M4	1.4 +/- 1.1	2.8 +/- 0.5	0.28 +/- 0.05
M5	3.2 +/- 1.1	3.0 +/- 0.5	0.28 +/- 0.05

485
486
487
488
489
490
491
492
493
494
495
496
497
498
499
500
501

Table 1: Relative sea level trends (mm/yr) recorded by the M3, M4 and M5 tide gauges (estimated with and without the seasonal cycles) as well as the GNSS-based vertical land motion (mm/yr) at the Senetosa site.

The M4 time series displays several gaps over the study period. In addition, the record (seasonal cycle not removed, Fig. 12a) shows a large positive anomaly in 2015, not seen by M3 neither M5. M3 has also a large gap in 2009/2010, as well as other gaps 2012 and at the end of the record. A suspect drop is also well visible in 2005 on Fig. 12b (seasonal cycle removed). Thus the M5 record seems the most reliable, even if the trends from M3 and M4 are close to M5 (see Table 1). The computed (relative) sea level trend (uncorrected for the VLM) is on the order of 2.8-3.8 mm/yr over the study period (seasonal cycle removed). If the GNSS VLM trend is accounted for, this range becomes 3.1-4.1 mm/yr. This value is significantly less than the altimetry-based sea level trends reported here in the last 4-5 km to the coast. On the other hand, the tide gauge trend agree well with the altimetry-based trends reported at distances greater than > 4 km from coast. While the reported altimetry-based sea level trend increase may disqualify our retracked sea level data in the vicinity of the coast, in



502

503 the next section we discuss the possibility that some coastal processes affect sea level in a
504 band of a few km from the coast while being attenuated very close to the shore where the tide
505 gauges (in particular M5) are located. .

506

507 **6. Small scale coastal processes**

508 Compared to deep-ocean sea level, sea level close to the coast can be impacted by various
509 small-scales processes resulting from the morphology of the coastline, the depth of the
510 continental shelf, the presence of a river estuary, etc. (Woodworth et al., 2019). Thus coastal
511 sea level may significantly differ from open ocean sea level over a large range of temporal
512 scales. In terms of trends, the open ocean sea level essentially results from processes affecting
513 the global mean sea level (mean ocean thermal expansion, land ice melt and land water
514 storage changes) (e.g., WCRP, 2018) and the superimposed regional variability (regional
515 changes in ocean thermal expansion, atmospheric loading and fingerprints due to the solid
516 Earth response to changing ice mass loads; Stammer et al., 2013). At the coast, in addition of
517 these two contributions, local variations in other processes may cause additional small-scale
518 sea level changes at interannual to decadal time scales, such as trapped Kelvin waves,
519 upwelling/downwelling effects, eddies, wind-generated waves and swells, shelf currents,
520 water density changes related with river runoff in estuaries (see Woodworth et al., 2019 for a
521 detailed discussion on forcing factors affecting sea level changes at the coast). Note that we
522 do not discuss vertical land motion here since our objective is to understand the observed
523 change in ‘geocentric’ sea level as measured by satellite altimetry.

524 In the case of Senetosa, river runoff and trapped Kelvin waves are not supposed to affect
525 coastal sea level. Could other processes like trends in wind-generated waves and coastal
526 currents explain the slow increase in sea level trend towards the coast? These are discussed
527 below.

528

529 **6.1 Effect of waves on SLA and SSB**

530 We first discuss the effect of waves. The contribution of wind-generated waves to coastal sea
531 level changes has been investigated in a number of recent studies (e.g., Melet et al., 2018,
532 Dodet et al., 2019). As thoroughly discussed in Dodet et al. (2019), wind-generated waves
533 have the capability to significantly change sea level variations at the coast, even at the time
534 scales of interest here. The shoaling and breaking of waves in the shelf shallow waters raises
535 the mean water level in the so-called near-shore and surf zones (last ~1 km to coast), a

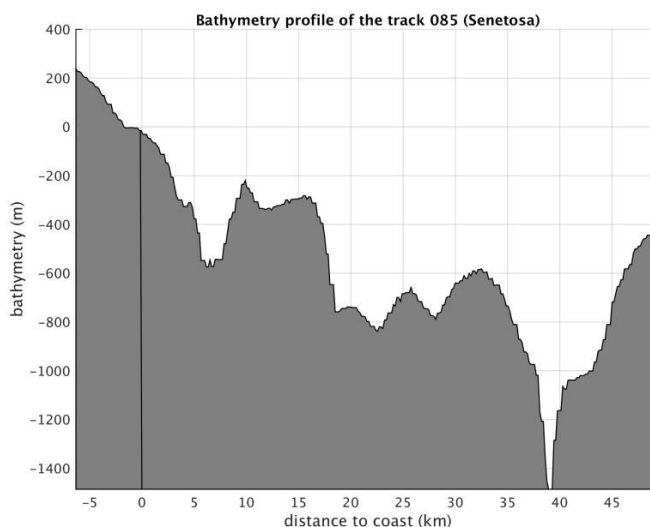


536

537 process called wave set-up. Wave set-up is proportional to offshore significant wave height,
538 and if the latter displays a temporal trend due to a trend in wind forcing, it may cause a sea
539 level trend in the coastal zone.

540 The relationship between offshore wave height and wave set-up is known empirically only
541 (Dodet et al., 2019). To first order, wave set-up is related to offshore SWH, wave period and
542 beach slope. The bathymetric profile along the Jason track 85 (from 45 km offshore to coast)
543 is shown in Fig. 13. We note an abrupt increase of more than 500 m in the last 5 km to coast,
544 corresponding to a slope of 0.1.

545



546

547

548 *Fig. 13: Bathymetric profile (meters) along Jason track 85 from 45 km offshore to coast*

549

550

551 If the bathymetric slope near Senetosa is known, it is not the case for other parameters
552 involved in the relationship between SWH and wave set-up. This is the case in particular for
553 beach soil characteristics, sediment size, etc. A large variety of formulations have been
554 proposed for this relationship, based on in situ observations collected at different coastal sites
555 (e.g., Dodet et al., 2019). However these are not necessarily applicable to our study case as
556 some local beach parameters are not known. But it is generally assumed that wave set up does
557 not exceed 20% of SWH. Thus, as a preliminary approach, we analyzed offshore SWH data
558 only, in order to highlight their temporal variability over our study time span.

559 For that purpose we considered wave field data from the ERA5 reanalysis
560 (<https://www.ecmwf.int/en/forecasts/datasets/reanalysis-datasets/era5>). The ERA5 reanalysis

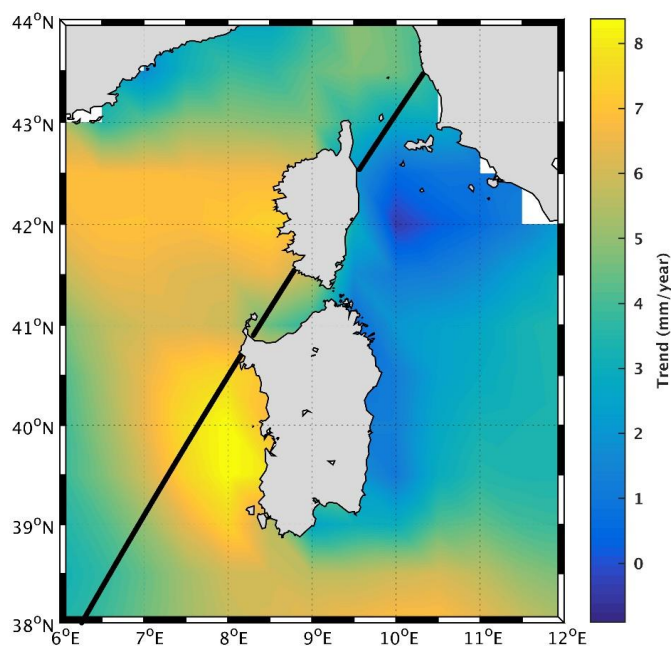


561

562 provides gridded SWH time series at monthly interval, from 1979-present, thus covering our
563 study period. The grid size resolution is 0.5 degree. Using this data set, we computed 2-D
564 SWH trends over 2002-2016, shown in Fig. 14. We note high positive wave height trends
565 west of Corsica and Sardinia over this period. Along the Jason track 85, in the vicinity of
566 Senetosia, the trend is on the order of 5 mm/yr.

567 From the above discussion, we deduce that wave set up would not contribute by more than 1
568 mm/yr to the coastal sea level trend. Noting in addition that wave set up would affect sea level
569 in the close vicinity of the coast only (i.e., not over 4-5 km distance, X. Bertin, and J. Wolf,
570 personal communications), we conclude that wave set up very unlikely explains the reported
571 coastal sea level trend.

572
573



574
575

576 *Fig. 14: Wave height trends (in mm/yr) over 2002-2016 in the western Mediterranean Sea*
577 *(data from ERA5 reanalysis)*

578

579 However, we further investigated the effect of waves on the ssb correction, hence on SLAs.
580 For that purpose, we computed the correlation between wave height time series and difference
581 in sea level between each 20 Hz altimetry point and a reference altimetry point located in the

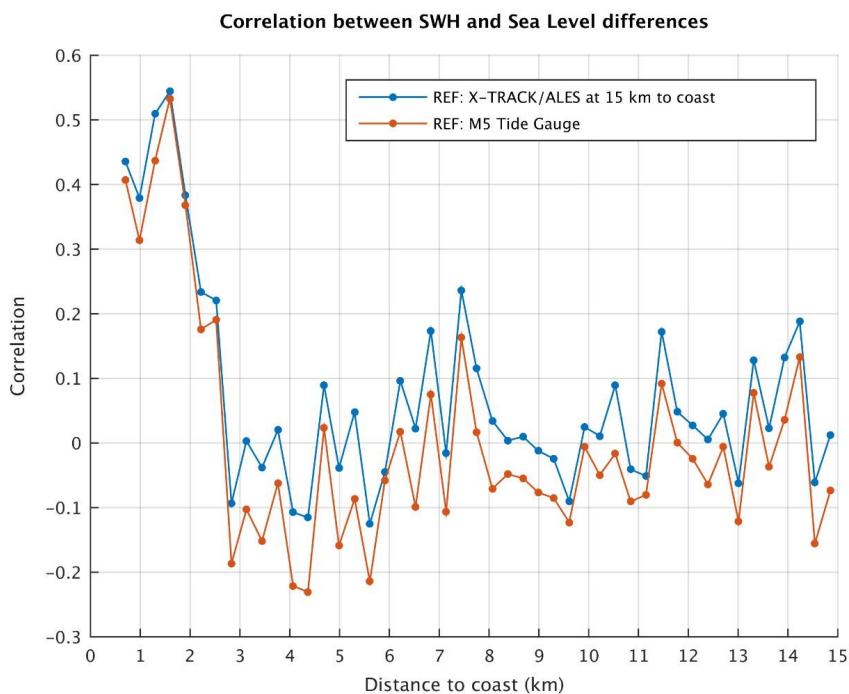


582

583 open ocean (chosen here at 15 km from the coast). We consider sea level differences in order
584 to remove the common signal affecting sea level close to the coast and offshore, i.e., the
585 global mean component and its superimposed regional variability. Data from the ERA5 grid
586 mesh closest to Senetosa were used. The correlation values are shown in Fig. 15 as a function
587 of distance to the coast. From a distance of ~3 km from the coast towards the deep sea, the
588 correlation is insignificant while it clearly increases from ~3 km to the coast. This suggests
589 that there is a link between the variations in waves and SLA variations in the 0-3 km domain
590 close to land.

591 We performed the same analysis but now using the M5 tide gauge record as reference (the M3
592 tide gauge record having too many data gaps). This is also shown in Fig. 15. Surprisingly, we
593 find exactly the same behavior of the correlation coefficient, i.e., no correlation offshore
594 (points located at distance > 3 km from coast) and an increase in correlation in the last 3 km
595 to the coast. This now suggests that waves affect SLA only in the domain 0-3 km but that at
596 the tide gauge site, waves have no influence. Obviously, this could be via the ssb correction
597 applied to SLA data.

598
599



600

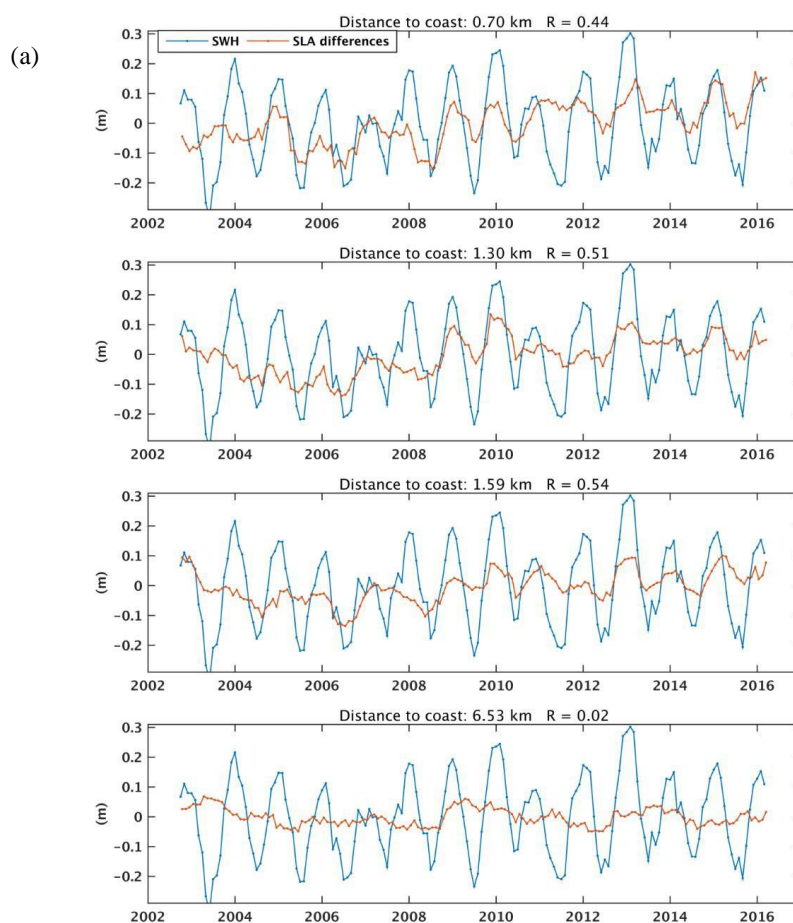
601

602 *Fig. 15: Correlation between the wave height (SWH) time series (from ERA5 grid mesh close*
603 *to Senetosa) and altimetry-based sea level difference time series between every 20 Hz point*
604 *and a reference point. (a) The reference time series corresponds to a point located at 15 km*
605 *from the coast. (b) The reference time series is the M5 tide gauge record.*
606

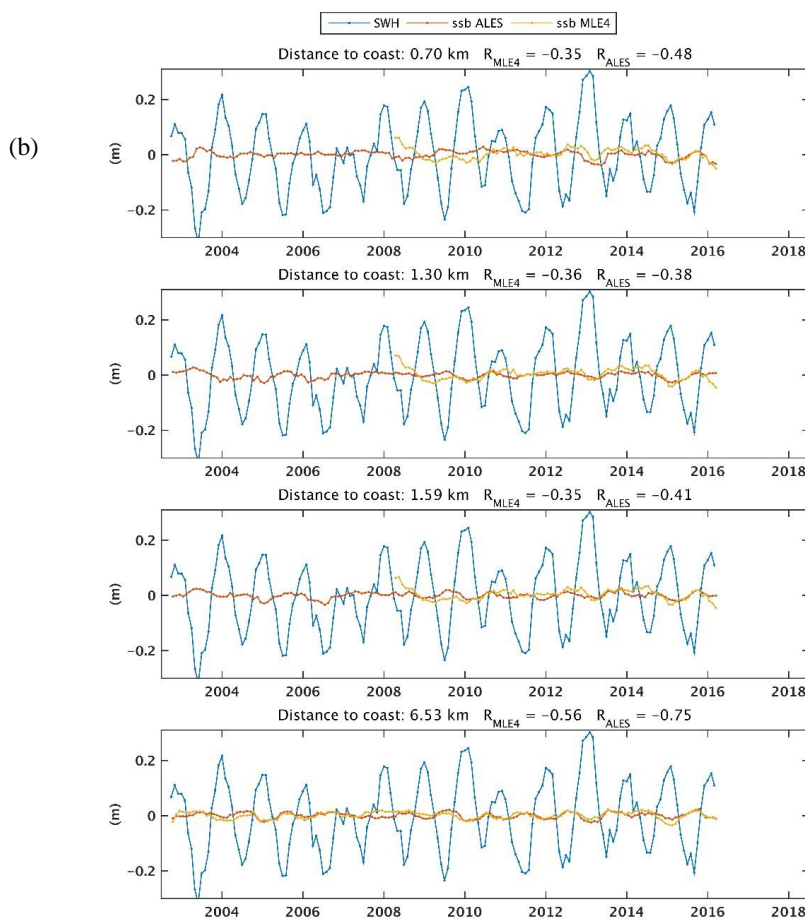
607 To illustrate this somewhat differently, Fig. 16a shows wave height time series superimposed
608 to altimetry-based difference in SLA time series (reference point at 15 km, as in Fig. 15) for a
609 few points located in the 0-3 km domain close to the coast and an additional point located
610 farther from the coast. Here again, data from the ERA5 grid mesh closest to Senetosa have
611 been considered for the calculation. The correlation between SWH and difference SLA time
612 series is indicated on each plot. We clearly see that it is significant only for points close to the
613 coast. Distant offshore points do not show such a correlation. Although the correlation is
614 dominated by the seasonal signal, Fig. 16a shows the two time series are also correlated at
615 interannual time scales. This clearly suggests that computed SLAs are impacted by waves in
616 the last few km to the coast on a broad range of time scales. We repeated this correlation
617 analysis but now using *ssb* (from both the ALES and MLE4 retrackings) instead of SLA
618 differences. The corresponding figure is shown in Fig. 16b.

619

620



621
622
623
624
625
626
627
628
629
630
631
632
633
634
635
636
637
638
639
640
641
642
643
644
645
646
647
648
649
650
651
652
653
654
655
656
657
658
659
660
661
662
663



664 Fig. 16: (a) Time series of ERA5-based wave height time series (blue curve) and of altimetry-
665 based SLA differences (orange curve) between 20 Hz points at different distances from coast
666 (indicated on each plot) and a reference point (located at 15 km). (b) same as (a) but using
667 ALES ssb instead of SLA differences. On Fig. 16b, MLE4 ssb are also shown for the Jason-2
668 time span (yellow curve). R is the correlation coefficient.

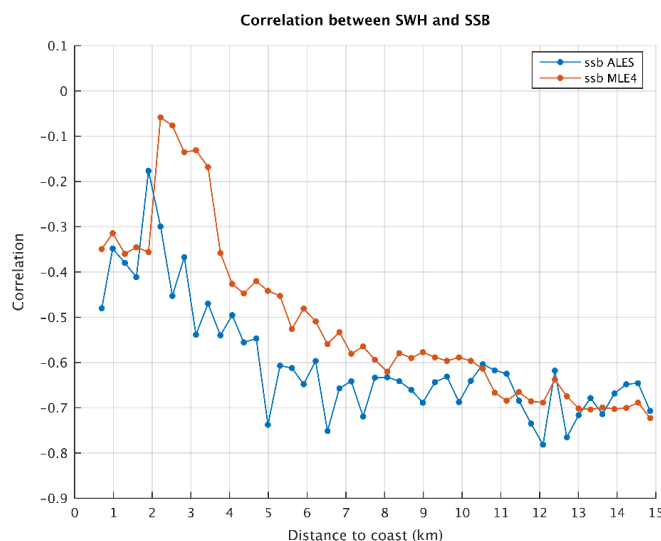
669 As expected ssb is correlated with wave height but the correlation decreases in the last few
670 km to the coast, suggesting that the relationship used to express the link between ssb and
671 SWH is less adapted in the coastal domain than in the open sea, possibly because of change of
672 wave properties. This is also illustrated in Fig. 17 that shows the correlation between ssb and
673 SWH as a function of distance to the coast (for both ALES ssb and MLE4 ssb). Between 1 km



674

675 and 4 km, the correlation between SWH and ssb decreases. Yet, it remains significant for
676 ALES ssb while very low for MLE4 ssb.

677



678

679

680 Fig. 17: Correlation between significant wave height (SWH) time series and ssb time series
681 between every 20 Hz point and a reference point.

682

683 We conclude from these tests, that the correlation between SLA and wave height at 20 Hz
684 points close to the coast is very likely due to imperfect ssb correction. Thus we can now
685 exclude any direct effect of waves (e.g., trend in wave set-up) as a candidate to explain the
686 SLA trend increase close to the coast. Are the reported SLA trends in the last few km to the
687 coast due to inadequate formulation of the relationship between SWH and ssb as the satellite
688 approaches the coast remains so far an open question. While we cannot exclude that the ssb
689 correction is imperfect close to the coast, it seems unlikely that it would produce such large
690 trends as those observed in the SLAs.

691

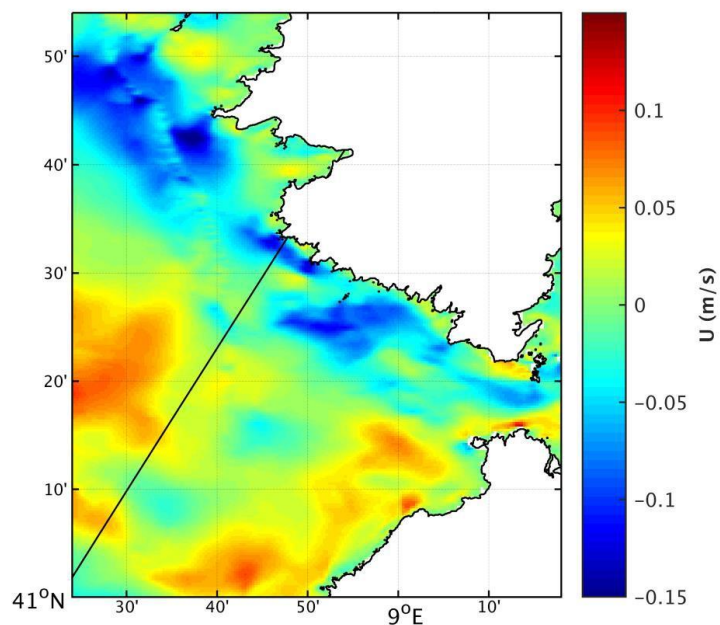
692 6.2. Effect of coastal currents and comparison with an ocean model

693 In this section we briefly address the effect of coastal currents on the SLAs. There are only
694 few published studies on the circulation in the Senetosa region (e.g., Bruschi et al., 1981,
695 Manzena et al., 1985, Cucco et al., 2012, Gerigny et al., 2015, Sciascia et al., 2019). These
696 indicate that the dominant characteristics of the circulation in the Corsica channel (Bonifacio
697 Straits) is a flow predominantly directed northward from the Tyrrhenian Sea to the Ligurian



698

699 Sea and that the water motion is mainly wind-driven. The study by Gerigny et al. (2015)
700 based on in situ measurements collected during a cruise in 2012 and use of a high-resolution
701 regional hydrodynamic model (MARS3D) shows that the circulation is mostly wind-driven.
702 The region is affected by westerly winds half of the year and strong easterly winds in winter.
703 The water circulation is highly dependent on this wind regime with often violent winds
704 generating strong local currents and mesoscale structures in the western part of the channel.
705 We have downloaded the currents data generated by the MARS3D model, a coastal
706 hydrodynamical model developed by IFREMER (Institut Français de Recherche pour
707 l'Exploitation de la Mer; Lazure and Dumas 2008). There is a high-resolution (400 m) version
708 available for the Corsica region, for the years 2014 to present
709 (<http://www.ifremer.fr/docmars/html/doc.basic.intro.html>). The model does not assimilate
710 altimetry data nor any other type of data. Because this dataset has only 2.5 years of overlap
711 with our study period, we cannot compute trends. However, to gain some insight on the
712 circulation configuration, we examined the currents pattern over the year 2014. In
713 agreement with the literature, we observed a strong zonal current during the winter months
714 close to Senetosa. An example of the zonal component of the barotropic current south of
715 Corsica is shown in Fig.18 for January 2014. We note a clear westward current along the
716 Senetosa coast. It is also worth noting that it does not extend to the shoreline, thus may not
717 influence tide gauge measurements.
718



719

720

721 *Fig.18: Barotropic current (zonal component) for January 2014 based on the MARS3D*
722 *hydrographic model. Blue color means westward current.*

723

724 We interpolated these current data (for January 2014) along the Jason track. This is shown in
725 Fig.19 as a function of distance to the coast. The current intensity is close to zero at distances >
726 5km from the coast. In the last 5 km to the coast, there is a steep intensity increase, exactly over
727 the same distance range as the SLA trend increase. Since the model resolution is ~400m, i.e.,
728 about the same resolution as the 20 Hz along-track SLAs, we find this result highly promising.

729

730

731

732

733

734

735

736

737

738

739

740

741

742

743

744

745

746

747

748

749

750

751

752

753

754

755

756

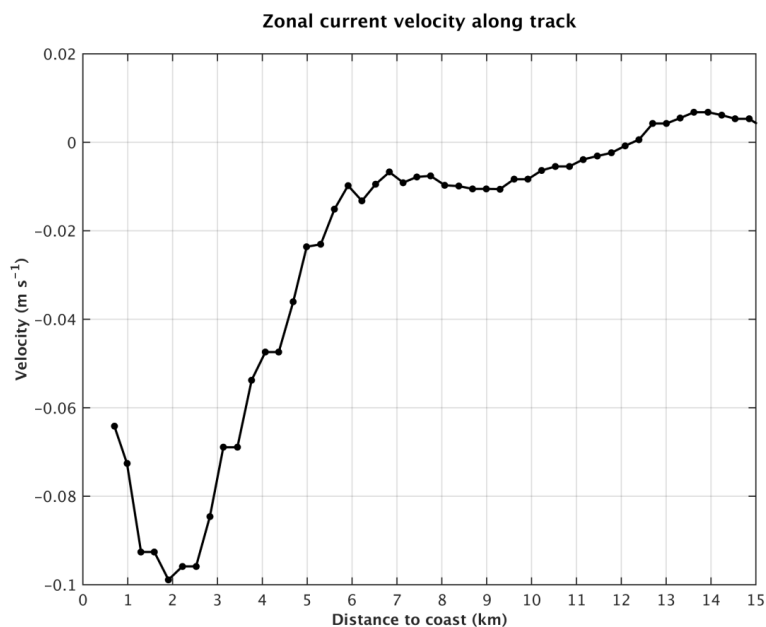
757

758

759

760

761



754 *Fig.19: Barotropic current (zonal component) for January 2014 based on the MARS3D*
755 *hydrographic model interpolated along the Jason track, as a function of distance to the*
756 *coast. Negative values mean westward current.*

757

758 Of course, we cannot extrapolate backward in time nor offer any solid conclusion so far. But we
759 cannot exclude that the observed sea level trend increase is linked to an increase in intensity of
760 this winter current during our study period. This obviously will need much deeper investigation,
761 at least over the time span of availability of the model data.



762

763 **7. Conclusion**

764 In this study, we have investigated the differences between coastal and deep ocean sea level
765 changes at the Senetosa site, using new ALES-based retracked sea level data from the Jason-1
766 and Jason-2 missions. We indeed observe a slow increase in sea level trend at short (< ~4-5
767 km) distance from the coast compared to offshore. A series of test shows that this behavior
768 does not result from artifacts due to spurious trends in the geophysical corrections applied to
769 the altimetry data, decreasing percentage of valid data, or errors in the intermission bias nor
770 errors in range estimates due to distorted radar waveforms.

771 Among the physical mechanisms able to explain the coastal trend increase in the study region,
772 we have first explored waves, then currents. We investigated the wave effect on sea level
773 along the Jason track and found that wave set up has a too small magnitude and is localized
774 too close to the shore to explain the observed continuous SLA trend increase in the last 4-5
775 km to the coast. On the other hand, the correlation reported between altimetry-based SLAs
776 and SWH very likely results from the imperfect ssb correction applied to the data.
777 Nevertheless, if less accurate in the coast vicinity, the ssb trend seems unable to explain the
778 reported SLA trend increase. We next investigated the effect of coastal currents. Using the
779 MARS3D high resolution model developed by IFREMER for coastal studies, we noted the
780 presence of a winter current elongated along the Senetosa coastline. Projection of this current
781 along the Jason track (for January 2014) shows a steep increase in intensity over exactly the
782 same distance to the coast as the SLA trend increase. This may be in indication of a current-
783 related origin. More studies are definitely needed to confirm the results presented here.
784 However, if further investigations confirm the effect of currents, it will be a demonstration
785 that small-scale processes acting in the vicinity of the coast may have the capability to make
786 coastal sea level changes drastically different from what we measure offshore with classical
787 altimetry.

788

789

790

791

Acknowledgements:

792 This study is a contribution to the ESA Climate Change Initiative (CCI+) Sea Level project.
793 Yvan Gouzenes is supported by an engineer grant in the context of this project (ESA SL_cci+
794 contract number 4000126561/19/I-NB). We thank a number of colleagues for very fruitful
795 discussions on the effect of waves on tide gauges and coastal sea level, in particular (by
796 alphabetic order) Angel Amores, Xavier Bertin, Svetlana Jevrejeva, Goneri Le Cozannet,
797 Marta Marcos, Judy Wolf and Phil Woodworth.



798

799

800 **References**

801

802 Ablain M., Legeais J.F., Prandi P., et al., 2017. Altimetry-based sea level, global and regional,
803 *Surveys in Geophysics*, 38, 7-31, <https://doi.org/10.1007/s10712-016-9389-8>.

804

805 Almar, R., E. Kestenare, J. Reyns, J. et al., 2015. Response of the Bight of Benin (Gulf of
806 Guinea, West Africa) coastline to anthropogenic and natural forcing, Part1: Wave climate
807 variability and impacts on the longshore sediment transport, *Continental Shelf Research*, 110,
808 48-59, <https://doi.org/10.1016/j.csr.2015.09.020>.

809 Birol F. and C. Delebecque, 2014. Using high sampling rate (10/20 Hz) altimeter data for the
810 observation of coastal surface currents: A case study over the northwestern Mediterranean
811 Sea, *J. Mar. Syst.*, <https://doi.org/10.1016/j.jmarsys.2013.07.009>.

812

813 Birol F., N.X Fuller, F. Lyard, et al., 2017. Coastal applications from nadir altimetry: example
814 of the X-TRACK regional products. *Advances in Space Research*, 59, 936-953,
815 <https://doi.org/10.1016/j.asr.2016.11.005>.

816

817 Bruschi A., Buffoni G., Elliott A.J., Manzella G., 1981. A numerical investigation of the
818 wind-driven circulation in the Archipelago of La Maddalena, *Oceanol. Acta*, 4, 3, 289-295.

819

820 Bonnefond, P., Exertier, P., Laurain, O., Ménard, Y., Orsoni, A., Jan, G., Jeansou, E., 2003a,
821 Absolute calibration of Jason-1and TOPEX/Poseidon altimeters in Corsica, in: Special Issue
822 on Jason-1 Calibration/ Validation, Part 1. *Mar. Geod.* 26(3-4), pp. 261-284,
823 <https://doi.org/10.1080/714044521>.

824

825 Bonnefond, P., Exertier, P., Laurain, O., Ménard, Y., Orsoni, A., Jeansou, E., Haines, B.J.,
826 Kubitschek, D.G., Born, G.H. Leveling sea surface using a GPS catamaran, 2003b, in:
827 Special Issue on Jason-1 Calibration/ Validation, Part 1. *Mar. Geod.* 26(3-4), 319-334,
828 <https://doi.org/10.1080/714044524>.

829

830 Bonnefond, P., Exertier, P., Laurain, O., Jan, G., 2010, Absolute calibration of Jason-1 and
831 Jason-2 altimeters in Corsica during the formation flight phase, in: Special Issue on Jason-2
832 Calibration/Validation, Part 1. *Mar. Geod.* 33(S1), 80-90,
833 <https://doi.org/10.1080/01490419.2010>.

834

835 Bonnefond, P., B. Haines and C. Watson. In Situ Calibration and Validation: A Link from
836 Coastal to Open-ocean altimetry, 2011, in Coastal Altimetry, chapter 11, pp 259-296, edited
837 by S. Vignudelli, A. Kostianoy, P. Cipollini, J. Benveniste, Springer, ISBN: 978-3-642-
838 12795-3. https://doi.org/10.1007/978-3-642-12796-0_11

839

840 Bonnefond, P., Exertier, P., Laurain, O., Guinle, ., F m nias, ., 201 , Corsica: A 20-Yr
841 Multi-Mission Absolute Altimeter Calibration Site, *Advances in Space Research*, Special
842 Issue « 25 Years of Progress in Radar Altimetry », <https://doi.org/10.1016/j.asr.2019.09.049>.

843

844 Church, J. A. et al., 2013: Sea Level Change. In: Climate Change 2013: The Physical Science
845 Basis. Contribution of Working Group I to the Fifth Assessment Report of the
846 Intergovernmental Panel on Climate Change [Stocker, T. F., D. Qin, G. K. Plattner, M.
847 Tignor, S. K. Allen, J. Boschung, A. Nauels, Y. Xia, V. Bex and P. M. Midgley (eds.)].



848

849 Cambridge University Press, Cambridge, United Kingdom and New York, NY, USA, 1137-
850 1216.

851 Cipollini P., J. Benveniste, F. Birol, et al., 2018. Satellite altimetry in coastal regions. In
852 ‘Satellite altimetry over the oceans and land surfaces’, Stammer & Cazenave Edts, CRC
853 Press, Taylor and Francis Group, Boca Raton, London, New York, pp 343-373,
854 <https://doi.org/10.1201/9781315151779-11>

855

856 Cucco A et al., 2012, A high-resolution real-time forecasting system for predicting the fate of
857 oil spills in the Strait of Bonifacio (western Mediterranean Sea), *Marine Pollution Bulletin*,
858 64, 1186-1200, doi:10.1016/j.marpolbul.2012.03.019.

859

860 Dieng, H., A. Cazenave, B. Meyssignac and M. Ablain, 2017: New estimate of the current
861 rate of sea level rise from a sea level budget approach. *Geophysical Research Letters*, 44 (8),
862 3744-3751, <https://doi.org/10.1002/2017GL073308>.

863

864 Dodet G., Melet A., Arduin F., Bertin X., Idier D. and Almar R., 2019. The contribution of
865 wind-generated waves to coastal sea level changes, *Surveys in Geophysics*, 40, 1563-1601,
866 <https://doi.org/10.1007/s10712-019-09557-5>.

867

868 Durand F., Piecuch C., Cirano M. et al., 2019. Impact of continental freshwater runoff on
869 coastal sea level, *Surveys in Geophysics*, 40:1437–1466, <https://doi.org/10.1007/s10712-019-09536-w>.

870

871

872 Gerigny O., Coudray S., Lapucci C., Tomasino C., Bisgambiglia P.A., Galgani F., 2015,
873 Small-scale variability of the current in the Strait of Bonifacio, *Ocean Dynamics*, 65, 8, 1165-
874 1182, <http://dx.doi.org/10.1007/s10236-015-0863-5>.

875

876 Lazure P and Dumas F, 2008, An external–internal mode coupling for a 3D hydrodynamical
877 model for applications at regional scale (MARS), *Advances in Water Resources*, 31:233-250,
878 doi:10.1016/j.advwatres.2007.06.010.

879

880 Legeais J.F., Ablain M., Zawadzki L. et al., 2018. An improved and homogeneous altimeter
881 sea level record from the ESA Climate Change Initiative, *Earth Syst. Sci. Data*, 10, 281-301,
882 <https://doi.org/10.5194/essd-10-281-2018>.

883

884 Léger F., F. Birol, F. Niño, M. Passaro, F. Marti and A. Cazenave, 2019, "X-Track/Ales
885 Regional Altimeter Product for Coastal Application: Toward a New Multi-Mission Altimetry
886 Product at High Resolution," IGARSS 2019 - 2019 IEEE International Geoscience and
887 Remote Sensing Symposium, Yokohama, Japan, 8271-8274,
888 <https://doi.org/10.1109/IGARSS.2019.8900422>.

889

890 Manzella G.M.R., 1985, Fluxes across the Corsica Channel and coastal circulation in the East
891 Ligurian Sea, North-Western Mediterranean, *Oceanol. Acta*, 8, 1, 29-35.

892

893 Marti F., Cazenave A., Birol F., Passaro, M. Leger F., Nino F., Almar R., Benveniste J. and
894 Legeais J.F., 2019, Altimetry-based sea level trends along the coasts of western Africa, *Adv.*
895 *in Space Res.*, published online 24 May2019, <https://doi.org/10.1016/j.asr.2019.05.033>.



896

32

- 897 Melet, A., Almar, R. and Meyssignac, B., 2016. What dominates sea level at the coast: a
898 case study for the Gulf of Guinea. *Ocean Dyn.* 66, 623–636,
899 <https://doi.org/10.1007/s10236-016-0942-2>.
- 900 Melet A., Meyssignac B. Almar R. et al., 2018. Under-estimated wave contribution to
901 coastal sea-level rise, *Nature Climate Change*, 8, 234–239, [https://doi.org/10.1007/s10236-](https://doi.org/10.1007/s10236-016-0942-2)
902 [016-0942-2](https://doi.org/10.1007/s10236-016-0942-2).
- 903 Nerem, R. S. et al., 2018: Climate-change–driven accelerated sea-level rise detected in the
904 altimeter era. *Proceedings of the National Academy of Sciences*,
905 <https://doi.org/10.1073/pnas.1717312115>.
906
- 907 Passaro M., Cipollini P., Vignudelli S. et al., 2014. ALES: A multi-mission subwaveform
908 retracker for coastal and open ocean altimetry. *Remote Sensing of Environment* 145, 173-189,
909 <https://doi.org/10.1016/j.rse.2014.02.008>.
- 910 Passaro M., Cipollini P., Benveniste J., 2015, Annual sea level variability of the coastal
911 ocean: the Baltic Sea-North Sea transition zone. *J Geophys Res Oceans* 120(4):3061–3078,
912 <https://doi.org/10.1002/2014JC010510>.
- 913 Passaro M., Zulfikar Adlan N. and Quartly G.D., 2018. Improving the precision of sea level
914 data from satellite altimetry with high-frequency and regional sea state bias corrections.
915 *Remote Sensing of Environment*, 245-254, <https://doi.org/10.1016/j.rse.2018.09.007>.
- 916 Piecuch C.G., Bittermann K., Kemp A.C. et al., (2018). River-discharge effects on United
917 States Atlantic and Gulf coast sea-level changes, *PNAS*, vol. 115, no. 30, 7729–7734,
918 <https://doi.org/10.1073/pnas.1805428115>.
- 919
- 920 Sciascia R., Magaldi M. and Vetrano A., 2019, Current reversal and associated variability
921 within the Corsica Channel: The 2004 case study, *Deep-Sea Research Part I*, 144, 39-51.
922
- 923 SROCC 2019: IPCC Special Report on the Ocean and Cryosphere in a Changing
924 Climate [H.-O. Pörtner, D.C. Roberts, V. Masson-Delmotte, P. Zhai, M. Tignor, E.
925 Poloczanska, K. Mintenbeck, A. Alegría, M. Nicolai, A. Okem, J. Petzold, B. Rama, N.M.
926 Weyer (eds.) et al.]. In press.
- 927 Stammer D, Cazenave A, Ponte RM, Tamisiea ME (2013) Causes for contemporary regional
928 sea level changes. *Annu Rev Mar Sci.* <http://doi.org/10.1146/annurev-marine-121211-172406>
929
- 930 Vignudelli S. , A. G. Kostianoy, P. Cipollini, and J. Benveniste (Eds.), 2011, Coastal
931 Altimetry, Springer, Berlin, <https://doi.org/10.1007/978-3-642-12796-0>.
- 932 The WCRP Global Sea Level Budget Group (2018). Global sea level budget, 1993-present.
933 *Earth Syst. Sci. Data*, 10, 1551–1590, <http://doi.org/10.5194/essd-10-1551-2018>
- 934 Woodworth P., Melet A., Marcos M. et al., 2019. Forcing Factors Causing Sea Level Changes
935 at the Coast, *Surveys in Geophysics*, <https://doi.org/10.1007/s10712-019-09531-1>.



936

33

937 Wöppelmann, G., and M. Marcos (2016), Vertical land motion as a key to understanding sea
938 level change and variability, *Rev. Geophys.*, 54, 64–92,
939 <https://doi.org/10.1002/2015RG000502>.